SPONSORED BY R&D SYSTEMS INC.

www.rndsystems.com/pathways

A Photon Turnstile Dynamically Regulated by One Atom

Barak Dayan *et al.*

Science **319**, 1062 (2008);
DOI: 10.1126/science.1152261

This copy is for your personal, non-commercial use only.

If you wish to distribute this article to others, you can order high-quality copies for your colleagues, clients, or customers by clicking here.

Permission to republish or repurpose articles or portions of articles can be obtained by following the guidelines here.

The following resources related to this article are available online at www.sciencemag.org (this information is current as of September 23, 2012):

Updated information and services, including high-resolution figures, can be found in the online version of this article at:
http://www.sciencemag.org/content/319/5866/1062.full.html

Supporting Online Material can be found at:
http://www.sciencemag.org/content/suppl/2008/02/21/319.5866.1062.DC1.html

This article has been **cited by** 54 article(s) on the ISI Web of Science

This article appears in the following **subject collections:**
Physics
http://www.sciencemag.org/cgi/collection/physics

Downloaded from www.sciencemag.org on September 23, 2012

Science (print ISSN 0036-8075; online ISSN 1095-9203) is published weekly, except the last week in December, by the American Association for the Advancement of Science, 1200 New York Avenue NW, Washington, DC 20005. Copyright 2008 by the American Association for the Advancement of Science; all rights reserved. The title *Science* is a registered trademark of AAAS.

A Photon Turnstile Dynamically Regulated by One Atom

Barak Dayan,[1] A. S. Parkins,[1]* Takao Aoki,[1]† E. P. Ostby,[2] K. J. Vahala,[2] H. J. Kimble[1]‡

Beyond traditional nonlinear optics with large numbers of atoms and photons, qualitatively new phenomena arise in a quantum regime of strong interactions between single atoms and photons. By using a microscopic optical resonator, we achieved such interactions and demonstrated a robust, efficient mechanism for the regulated transport of photons one by one. With critical coupling of the input light, a single atom within the resonator dynamically controls the cavity output conditioned on the photon number at the input, thereby functioning as a photon turnstile. We verified the transformation from a Poissonian to a sub-Poissonian photon stream by photon counting measurements of the input and output fields. The results have applications in quantum information science, including for controlled interactions of single light quanta and for scalable quantum processing on atom chips.

The charge and spin degrees of freedom of massive particles have relatively large long-range interactions, which enable nonlinear coupling between pairs of atoms, ions, electrons, and diverse quasi-particles. An early example for electrons is the observation of Coulomb blockade, in which charge transport through small metallic and semiconductor devices occurs electron by electron (*1*–*3*). Among diverse applications for such strong interactions, quantum information science (QIS) relies on large coherent couplings for the implementation of quantum computation, communication, and metrology (*4*).

Whereas electrons interact directly via Coulomb repulsion, photons have vanishingly small cross sections for direct coupling. Instead, photon interactions must be mediated by a material system. Even then, typical materials produce photon-photon coupling rates that are orders of magnitude too small for nontrivial dynamics with individual photon pairs. The leading exception to this state of affairs is cavity quantum electrodynamics (cQED), where strong interactions between light and matter at the single-photon level have enabled a wide set of scientific advances, including single atoms coupled to optical and microwave resonators (*5*–*8*), quantum dots paired with micropillars and photonic bandgap cavities (*9*, *10*), and Cooper pairs interacting with superconducting resonators (*11*, *12*).

Indeed, in analogy with Coulomb blockade for electrons (*1*–*3*), photon-photon interactions in a nonlinear optical cavity were proposed to realize photon blockade (*13*), for which a first photon within an optical system blocks the transmission of a second photon, leading to an orderly output of photons one by one. The initial observation of photon blockade (*14*) for an atomic system used a Fabry-Perot cavity containing one atom strongly coupled to the cavity field, for which the underlying blockade mechanism was the quantum anharmonicity of the ladder of energy levels for the composite atom-cavity system (*15*). Resonant absorption of a first photon to reach the lowest energy eigenstate blocks the absorption of a second photon, because transitions to higher-lying eigenstates are detuned from resonance by the strong interaction of atom and photon. Photon blockade has also been investigated within the context of a photon turnstile (*16*) and has been realized for diverse semiconductor systems (*10*) because of anharmonicity of the photoluminescence spectrum.

In these examples (*10*, *14*–*16*), as well as the original work in (*13*) and extensions thereof (*17*–*19*), photon blockade arises as a struc-

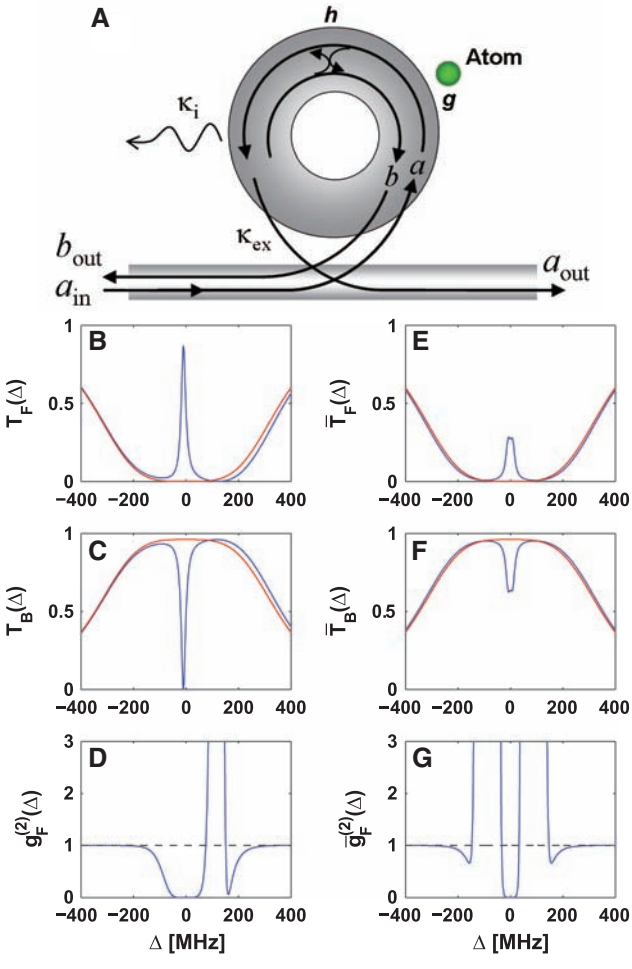

Fig. 1. (**A**) Schematic of microtoroidal resonator and fiber coupler (*20*, *22*). An atom interacts at rate g with the evanescent fields of two internal modes (a and b), which are coupled by scattering at rate h. The input a_{in} is driven by a coherent probe E_p of frequency ω_p, whereas b_{in} is in a vacuum state. (**B** to **G**) Theoretical results from our model (*24*). (B) to (D) Atomic localization with well-defined azimuthal phase $\varphi = \pi/2$. (B) and (C) Transmission spectra for the steady-state forward flux $T_F(\Delta) = \langle a_{out}^{+} a_{out}\rangle / \langle a_{out}^{+} a_{out}\rangle_{\Delta>>\kappa}$ and backward flux $T_B(\Delta) = \langle b_{out}^{+} b_{out}\rangle / \langle a_{out}^{+} a_{out}\rangle_{\Delta>>\kappa}$ as functions of probe detuning $\Delta = \omega_C - \omega_p$. (D) Steady-state intensity correlation function $g_F^{(2)}(\Delta) = \langle (a_{out}^{+})^2 (a_{out})^2\rangle / \langle a_{out}^{+} a_{out}\rangle^2$ for the forward flux. (E) to (G) Random atomic positions, with an average over $0 \le \varphi < 2\pi$. (E) and (F) Average steady-state transmission spectra $\bar{T}_F(\Delta), \bar{T}_B(\Delta)$. (G) Average steady-state intensity correlation function $\bar{g}_F^{(2)}(\Delta)$. In all frames, the red curves are for no atom ($g_0 = 0$), whereas the blue curves are with one atom coupled as illustrated in (A). The parameters for all plots (B) to (G) are $(g_0, \kappa_i, h, \gamma)/2\pi =$ (70,5,250,1) MHz with $\kappa_{ex} = \kappa_{ex}^{cr}$. For $\varphi = 0$, the plots are identical to those in (B) to (D) with the replacement $\Delta \rightarrow -\Delta$.

[1]Norman Bridge Laboratory of Physics, 12-33, California Institute of Technology, Pasadena, CA 91125, USA. [2]T. J. Watson Laboratory of Applied Physics, California Institute of Technology, Pasadena, CA 91125, USA.

*Present address: Department of Physics, University of Auckland, Auckland, New Zealand.

†Present address: PRESTO, Japan Science and Technology Agency, Saitama, Japan.

‡To whom correspondence should be addressed. E-mail: hjkimble@caltech.edu

Downloaded from www.sciencemag.org on September 23, 2012

tural effect due to anharmonic energy spectra for multiple excitations. The anharmonicity can be exploited to regulate photon transmission [refer to the level diagram in figure 1 of (*14*)] or, alternatively, to spectrally isolate emission events arising from single excitations [as illustrated in the schematic for biexciton decay in figure 1 of (*10*)].

In contrast to transport governed by structure, we describe observations of photon blockade in which photon transport is regulated dynamically by the conditional state of one intracavity atom, leading to an efficient mechanism that is insensitive to many experimental imperfections. As illustrated in Fig. 1, an atom interacting with the fields of a microtoroidal resonator (*20*) regulates the photon statistics of light transmitted and reflected by the resonator. This regulation is achieved by way of an interference effect involving the directly transmitted optical field, the intracavity field in the absence of the atom, and the polarization field radiated by the atom, with the requisite nonlinearity provided by the quantum character of the emission from one atom. Detection of an initial photon in the forward-propagating transmission results in subsequent photons from the incident flux being rerouted. This mechanism requires only that the intracavity atomic absorption be large and thus is robust against variations in atomic coupling. For fiber coupling to and from a microtoroidal resonator (*21*, *22*), we achieved high efficiency for the transport of photons through the turnstile.

Our investigation relied on measurements of photon correlations based on the normalized intensity correlation function $g_F^{(2)}(\tau)$ for the forward-propagating transmitted light (*23*). The incident field (which approximates a coherent state) has $g^{(2)}(\tau) = 1$, corresponding to a Poisson distribution for photon number independent of time delay τ. An ideal photon turnstile would achieve $g_F^{(2)}(0) = 0$ in correspondence to the state of a single photon. More generally, $g_F^{(2)}(0) < 1$ represents a nonclassical effect with the variance in photon number reduced below that of the incident field. For continuous illumination, $g_F^{(2)}(\tau)$ regresses to steady state over a time τ_B, with photon transmissions separated by time intervals $\Delta t >> \tau_B$ being statistically independent. The observation $g_F^{(2)}(0) < g_F^{(2)}(\tau)$ represents photon antibunching; photons are transported one by one through the turnstile without neighbors in time.

The mechanism responsible for photon regulation in our microtoroidal resonator is explained in more detail in Fig. 1. The basic model underlying this analysis is that of a single two-state atom coupled to a resonant cavity, namely the Jaynes-Cummings model extended to incorporate two cavity modes and to include damping by way of reservoir couplings (*24*). As depicted in Fig. 1A, the two internal counterpropagating modes a and b of the toroidal resonator have common frequency ω_C in the absence of scattering. These modes are coupled because of scattering with strength h. The field decay rate for the resonator modes is $\kappa = \kappa_i + \kappa_{ex}$, where κ_i represents intrinsic losses and κ_{ex} describes extrinsic loss due to (adjustable) coupling of the modes to the fiber coupler (*21*, *22*).

We consider an impedance-matched input (that is, critical coupling) for which κ_{ex} is set to $\kappa_{ex}^{cr} = \sqrt{\kappa_i^2 + h^2}$ and the resonator excited with probe detuning $\Delta \equiv \omega_C - \omega_p = 0$. In this case, interference between the cavity field a and the input field a_{in} results in zero flux in the forward direction, $\langle a_{out} \rangle = 0$, where $a_{out} = a_{in} + \sqrt{2\kappa_{ex}}\, a$. The incident flux $|E_p|^2$ appears in the backward direction b_{out} for low internal loss $\kappa_i << \kappa_{ex}$, as shown by the (normalized) probe spectra $T_F(\Delta), T_B(\Delta)$ for the forward- and backward-propagating fields a_{out} and b_{out} in Fig. 1, B and C, with $T_F(\Delta = 0) = 0$ whereas $T_B(\Delta = 0) \approx 1$ (red curves).

An atom near the external surface of the toroid has coherent interactions with the evanescent components of modes a and b that modify T_F and T_B. The fundamental description of these interactions is in terms of normal modes $A = (a + b)/\sqrt{2}$ and $B = (a - b)/\sqrt{2}$, which have mode functions $\psi_{A,B}(\rho, \varphi, z) = f(\rho, z)\{\cos(\varphi), \sin(\varphi)\}$ that are standing waves around the circumference φ of the toroid, with ρ the radial distance from the surface and z the vertical coordinate (*24*). The rate of coherent coupling of an atom to the A and B modes is given by $g_{A,B} = g_0\, \psi_{A,B}(\rho, \varphi, z)$, where for the geometry of our current resonator, we calculate that $g_0/2\pi \approx 95$ MHz (*20*).

Figure 1 shows examples of theoretical probe spectra $T_F(\Delta), T_B(\Delta)$ in the presence of an atom (blue curves) with atom-cavity detuning $\Delta_{AC} \equiv \omega_A - \omega_C = 0$ and for parameters relevant to our current experiment. Relative to the case with $g_0 = 0$ (no atom), there is now a sharp central feature around $\Delta = 0$ associated with atom absorption (*25*), where the width Γ of this feature exceeds the free-space radiative rate γ due to enhanced coupling to the cavity [equation 15 in (*24*)]. For normally ordered

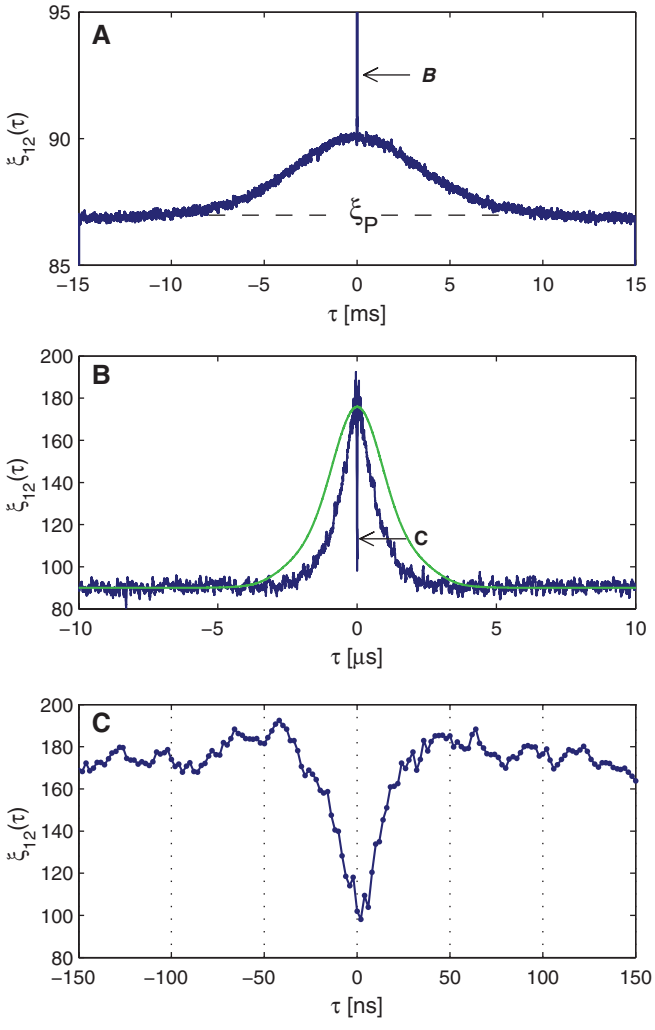

Fig. 2. Cross correlation $\xi_{12}(\tau)$ between photon counts at detectors D_1 and D_2 for the forward flux $\langle a_{out}^{+} a_{out} \rangle$ as a function of time offset τ. (**A**) The broad increase in $\xi_{12}(\tau)$ above the background level ξ_P is the envelope of atom transit events as a cloud of cold Cs atoms falls past the toroidal resonator. (**B**) The center feature indicated by the arrow in (A) is shown on an expanded time scale, revealing the average profile for individual atom transits. For comparison, the green curve is from the cross correlation of $P_1(t)$,$P_2(t+\tau)$ in Fig. 3A. (**C**) The center dip marked by the arrow in (B) is expanded further in τ to reveal a dip in joint detection events due to photon blockade by the atom-cavity system during the atom transit.

Downloaded from www.sciencemag.org on September 23, 2012

expectation values, the following replacements can be made (*24*)

$$a_{out} \rightarrow \alpha_0 + \alpha_-\sigma_-,\ b_{out} \rightarrow \beta_0 + \beta_-\sigma_- \qquad (1)$$

where σ_- is the lowering operator for atomic transitions, α_0, β_0 are c numbers derived for the empty cavity with no atom, and $(\alpha_-, \beta_-) \propto g_0$ describes the atom-cavity interaction. For critical coupling, $\alpha_0(\Delta_p \approx 0) \approx 0$, and the steady-state flux $\langle a^+_{out} a_{out}\rangle$ derives principally from the contribution of the atom, given by the term $\alpha_-\sigma_-$ in Eq. 1. In contrast, β_0 is nonzero near critical coupling, with the output b_{out} then determined by the coherent sum of contributions from the terms β_0 and $\beta_-\sigma_-$. For the particular case of atomic interaction with a single normal mode (such as $\varphi = \pi/2$) as in Fig. 1, B to D, these considerations lead to a transmission spectrum for the forward-propagating light a_{out} for which $T_F(\Delta_p \approx 0) \approx 1$, whereas for the backward light b_{out}, $T_B(\Delta_p \approx 0) \approx 0$.

Photon blockade arises in this setting as follows. With critical coupling, $\alpha_0 = 0$, so that a first photon transmitted into a_{out} can originate only from the atom (that is, the term $\alpha_-\sigma_-$ in Eq. 1). This emission projects the atom into its ground state, from which a second emission cannot occur ($\langle\sigma^2_+\sigma^2_-\rangle = 0$) (*26*, *27*). A second photon cannot be transmitted until the atomic state regresses to a steady state, which occurs over a time interval set by the cavity-enhanced emission rate Γ.

This qualitative prediction is substantiated in Fig. 1D from a calculation of the intensity correlation function $g^{(2)}_F(\tau = 0)$ for a_{out}. Around $\Delta = \omega_C - \omega_p = 0$, $g^{(2)}_F(0) \approx 0$ as expected for photon blockade. As suggested by Fig. 1C, photons arriving during an initial transmission event will be rerouted to the backward-propagating field b_{out}, so that photon bunching should be expected for b_{out}, as is indeed the case for $g^{(2)}_B(\tau = 0)$ (fig. S3).

Overall, for the conditions considered in Fig. 1, B to D, the atom-cavity system functions as a photon turnstile, with single photons transmitted into a_{out} and excess photons reflected into b_{out}. Conditioned on a first transmission event, the transmission characteristics of the system switch from those in Fig. 1, B and C, for the case $g_0 \neq 0$ to those for $g_0 = 0$. That is, a first photon transmitted triggers the change $\{T_F(\Delta \approx 0) \approx 1, T_B(\Delta \approx 0) \approx 0\}$ for $g_0 \neq 0 \rightarrow \{T_F(\Delta \approx 0) \approx 0, T_B(\Delta \approx 0) \approx 1\}$ with $g_0 = 0$, with regression back to the case $g_0 \neq 0$ occurring on a time scale τ_B.

The case of atomic localization at fixed ϕ as in Fig. 1, B to D, is not realistic for the experiment we performed. Hence, in Fig. 1, E to G, we present corresponding results averaged over the azimuthal angle φ (that is, for single-atom interactions but each at a random location in φ). The dominant effect is a reduction in the contrast for transmission and reflection. However, the atom-cavity system still functions effectively as a photon turnstile for the forward flux transmitted into a_{out}, with $\bar{g}^{(2)}_F(0) \approx 0$ at $\Delta = 0$, where $\bar{g}^{(2)}_F$ denotes an azimuthal average. For further discussion, see (*24*).

Our experiment to investigate these effects was similar to the setup shown in figure 1 of (*20*), with further details given in section I of (*24*). The principal difference between the depiction in Fig. 1A and the actual experiment is that individual Cs atoms were not trapped in the evanescent field of the toroid, but rather fell along z and transited through the evanescent field of the resonator. The toroidal resonator was monolithically fabricated from SiO_2 on a Si chip (*28*), had major diameter $D \approx 25$ μm and minor diameter $d \approx 6$ μm, and was located within a chamber at ultrahigh vacuum. From measurements of atom transit events as functions of atom-cavity detuning Δ_{AC} and intracavity photon number $\langle n\rangle$, we determined a single effective coupling strength $g_{eff}/2\pi \approx 70$ MHz (*24*), where ω_A corresponds to the $6S_{1/2}, F = 4 \rightarrow 6P_{3/2}, F' = 5$ transition in atomic Cs.

In contrast to our report in (*20*), we were not in the strong coupling limit of cQED, specified by $g_{eff} >> (\kappa^{cr}, \gamma_\perp)$, because the rate of decay for the cavity field was $\kappa^{cr}/2\pi = (165 \pm 15)$ MHz, whereas the free-space rate of decay of the atomic polarization was $\gamma_\perp/2\pi = 2.6$ MHz. Rather, the conditions were more appropriate to the "bad-cavity"

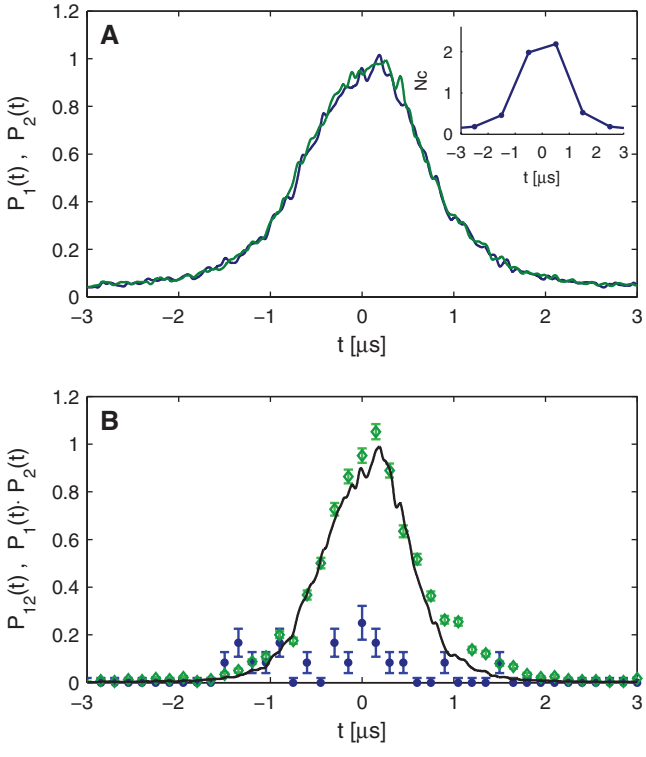

Fig. 3. Single $P_{1,2}(t)$ and joint $P_{12}(t)$ event probabilities versus time t around the center of transit events. (**A**) $P_1(t)/P_1(0)$ and $P_2(t)/P_2(0)$, where $P_1(0) = 2.88 \times 10^{-3}$, $P_2(0) = 2.80 \times 10^{-3}$. The inset shows the average number of counts N_c recorded during a transit for time bins $\delta t = 0.5$ μs. (**B**) $P_{12}(t)/[P_1(0)P_2(0)]$ (blue circles) and $[P_1(t)P_2(t)]/[P_1(0)P_2(0)]$ (black trace). There is a clear nonclassical suppression $P_{12}(t) < P_1(t)P_2(t)$. The green diamonds are the average of $P_{12}(t, t \pm \tau) \equiv \langle p_1(t)p_2(t + \tau)\rangle / \langle p_1(t)\rangle\langle p_2(t + \tau)\rangle$ for 26 ns $\leq \tau \leq$ 44 ns and demonstrate that emission events become statistically independent for $\tau > \tau_B$.

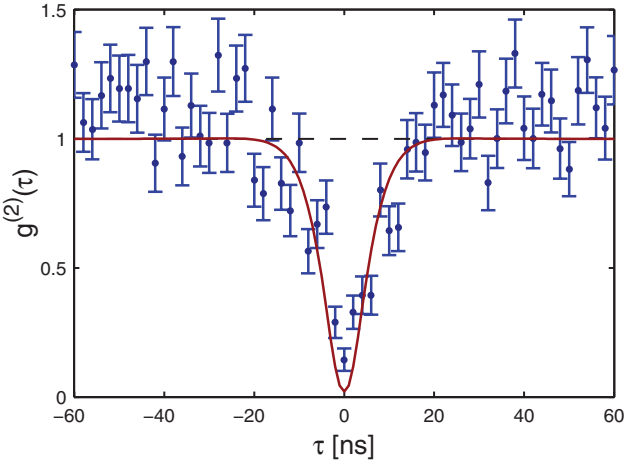

Fig. 4. Intensity correlation function $g^{(2)}(\tau)$ versus time delay τ for individual atomic transit events. $g^{(2)}(\tau)$ exhibits photon antibunching $g^{(2)}(0) < g^{(2)}(\tau)$, and sub-Poissonian photon statistics $g^{(2)}(0) = (0.14 \pm 0.04) < 1$, over an interval $\Delta\tau \approx 6$ ns (half width at half maximum) due to the operation of the atom-cavity system as a photon turnstile. The red trace is from our theoretical model.

Downloaded from www.sciencemag.org on September 23, 2012

limit, for which $\kappa^{cr} >> (g_{eff})^2/\kappa^{cr} >> \gamma_\perp$ (*25*). Other measured parameters for our system were $(\kappa_i, \kappa_{ex})/2\pi = (75, 90)$ MHz for the case of critical coupling.

For critical coupling with $\Delta \approx 0 \approx \Delta_{AC}$, we directed the forward flux for a_{out} (Fig. 1A) to two single-photon counters $D_{1,2}$ (fig. S1), with the outputs $C_{1,2}(t_i)$ from these detectors being time-stamped and stored for time bins $\delta t = 2$ ns for each value t_i. From raw records for $C_{1,2}(t_i)$, we directly computed the cross correlation $\xi_{12}(\tau) = \sum_i \langle C_1(t_i) C_2(t_i + \tau)\rangle$, with an example given in Fig. 2. Clearly evident in Fig. 2A is a broad bump of width $\Delta\tau_{cloud} \approx 7.5$ ms, corresponding to the overall envelope for transit events as the cloud of cold atoms falls past the toroid. The observed value for $\Delta\tau_{cloud}$ is in good agreement with the value of ~7 ms expected for our geometry (*24*). The pedestal at level ξ_P in Fig. 2A arose from background counts and was unchanged in the absence of atoms.

The central 20-μs interval in Fig. 2A is expanded in Fig. 2B to display a peak of full width $\Delta\tau_{transit} \approx 2$ μs that arises from transit events for individual atoms falling through the evanescent field of the toroid. Each atom experiences a time-varying coupling $g_0(\rho, \varphi, vt)$, where v is the atomic velocity in the z direction, leading to a temporal variation in the forward flux $T_F \propto \langle a_{out}^+ a_{out}\rangle$. Again, the observed time dependence is in accord with a theoretical model based on the calculated mode function for our toroid and the known atomic velocity v [see figure 3D in (*20*)].

Finally, the central 300-ns interval in Fig. 2B is expanded in Fig. 2C to reveal a dip in $\xi_{12}(\tau)$ around $\tau = 0$, corresponding to a paucity of coincidence counts between detectors D_1 and D_2 over an interval $\Delta\tau \approx 22$ ns (full width at half maximum). This suppressed probability for joint detection agrees with that expected from the analysis in Fig. 1 for a photon turnstile. However, independent of any purported microscopic mechanism, the results presented in Fig. 3C for $\xi_{12}(\tau)$ represent a prima facie observation of nonclassical light from the toroid, because $\xi_{12}(0) < \xi_{12}(\tau)$ (*23*). However, these results do not exhibit sub-Poissonian photon statistics. $\xi_{12}(0)$ does not drop below the level of the pedestal ξ_P shown in Fig. 2, A and B, because of the random arrival of atoms into the cavity mode (*29*).

Figure 2 is from an unconditional analysis of the records of photo counts $C_{1,2}(t_i)$. Because we could identify transit events for single atoms with high statistical confidence (*20*, *24*), we next performed an analysis conditioned on the presence of an atom. As described in section II of (*24*), for individual atomic transits recorded by detectors $D_{1,2}$, we derive the probabilities $p_{1,2}(t_i)$ and $p_{12}(t_i)$ for single and joint detections at $D_{1,2}$ during an atomic transit.

Figure 3A displays the single-event probabilities $P_{1,2}(t) \equiv \langle p_{1,2}(t)\rangle$ as functions of time t around the center $t = 0$ of the transit events with time bins of duration $\delta t = 2$ ns. The time dependence for $P_{1,2}(t)$ agrees with an independent estimate based on our cavity mode and the atomic velocity. The assertion that the peak in Fig. 3A arises predominantly from actual transit events is further supported by a comparison with the central feature in Fig. 2B.

Figure 3B presents results for the photon statistics for these transit events, now with $\delta t =$ 150 ns. The joint probability $P_{12}(t) \equiv \langle p_1(t) p_2(t)\rangle$ lies well below the level set by $P_1(t)P_2(t)$, violating the Cauchy-Schwarz inequality with $P_{12} < P_1 P_2$. Over the central 1-μs interval, we find that $P_{12}/P_1P_2 = (0.135 \pm 0.033) < 1$. In agreement with our theoretical analysis, an atomic transit event regulates the photon statistics of the output field, with a_{out} becoming markedly sub-Poissonian because of the atom-cavity interaction in the fashion of a photon turnstile.

Final support for this interpretation comes from Fig. 4, where we present measurements of the intensity correlation function $g^{(2)}(t, \tau) \equiv \langle p_1(t) p_2(t + \tau)\rangle / \langle p_1(t)\rangle\langle p_2(t + \tau)\rangle$. For times t_0 such that $-0.4\ \mu s \le t_0 \le +0.4\ \mu s$ around the center of the transit events in Fig. 3, $g^{(2)}(\tau) \equiv g^{(2)}(t_0, \tau)$ exhibits clear antibunching, as well as sub-Poissonian photon statistics. The full trace in Fig. 4 is from the steady-state solution to the master equation from our theoretical model, which has been averaged over the azimuthal angle φ [section VIII of (*24*)]. All parameters for this comparison were determined from independent measurements, including the effective coupling strength g_{eff}, which was used for the theoretical trace in Fig. 4. The agreement between theory and experiment is evidently quite reasonable. In particular, photon blockade persists over a time τ_B set by the cavity-enhanced atomic decay rate Γ, which is approximately given by $\tau_B \approx 2.5/\Gamma \approx 7$ ns for the parameters of our experiment [eq. 16 of (*24*)], in good agreement with $\Delta\tau \approx 6$ ns in Fig. 4.

Our results represent an observation of manifestly quantum (nonclassical) fields for cQED with single atoms and microresonators. The underlying dynamical mechanism for photon blockade is quite robust against many experimental imperfections, including variations in the coupling $g(\vec{r})$, requiring only that $g^2/\kappa^{cr}\gamma_\perp > 1$. For comparison, in our experiment $(g_{eff})^2/\kappa^{cr}\gamma_\perp \approx 11$. This mechanism is also robust against stronger excitation; numerical solutions of the full master equation show that the turnstile effect persists for an intracavity photon number up to the order of unity in the absence of an atom. Moreover, the measured throughput efficiency ζ for single photons [$T_F(\Delta = 0)$ in Fig. 1, B and E] reaches $\zeta \approx 25\%$ during single-atom transit events. Our theoretical analysis suggests that it should be possible to achieve $\zeta > 90\%$, thereby realizing an efficient photon turnstile for which an input field is sorted by photon number into forward- and backward-propagating output fields with small loss. By operating in a pulsed domain, investigations of photon collisions become possible, as well as quantum nondemolition detection. Because our toroidal resonators are lithographically fabricated with input-output coupling via optical fiber (*22*), our experiment provides an important first step into the quantum domain to implement scalable atom-cavity systems, including for quantum logic with photons (*30*) and for quantum processes on atom chips (*31*).

References and Notes

1. T. A. Fulton, G. J. Dolan, *Phys. Rev. Lett.* **59**, 109 (1987).
2. M. A. Kastner, *Rev. Mod. Phys.* **64**, 849 (1992).
3. K. K. Likharev, *Proc. IEEE* **87**, 606 (1999).
4. P. Zoller *et al.*, *Eur. Phys. J. D* **36**, 203 (2005).
5. R. Miller *et al.*, *J. Phys. B At. Mol. Opt. Phys.* **38**, S551 (2005).
6. T. Wilk, S. C. Webster, A. Kuhn, G. Rempe, *Science* **317**, 488 (2007).
7. H. Walther, *Fortschr. Phys.* **52**, 1154 (2004).
8. J. M. Raimond *et al.*, *J. Phys. B At. Mol. Opt. Phys.* **38**, S535 (2005).
9. For a review, see (*32*).
10. For a review, see (*33*).
11. J. Majer *et al.*, *Nature* **449**, 443 (2007).
12. M. A. Sillanpää, J. I. Park, R. W. Simmonds, *Nature* **449**, 438 (2007).
13. A. Imamoglu *et al.*, *Phys. Rev. Lett.* **79**, 1467 (1997).
14. K. M. Birnbaum *et al.*, *Nature* **436**, 87 (2005).
15. L. Tian, H. J. Carmichael, *Phys. Rev. A* **46**, R6801 (1992).
16. J. Kim *et al.*, *Nature* **397**, 500 (1999).
17. P. Grangier, D. F. Walls, K. M. Gheri, *Phys. Rev. Lett.* **81**, 2833 (1998).
18. M. J. Werner, A. Imamoglu, *Phys. Rev. A* **61**, 011801 (1999).
19. S. Rebić, A. S. Parkins, S. M. Tan, *Phys. Rev. A* **65,** 043806 and 063804 (2002).
20. T. Aoki *et al.*, *Nature* **443**, 671 (2006).
21. M. L. Gorodetsky, A. D. Pryamikov, V. S. Ilchenko, *J. Opt. Soc. Am. B* **17**, 1051 (2000).
22. S. M. Spillane, T. J. Kippenberg, O. J. Painter, K. J. Vahala, *Phys. Rev. Lett.* **91**, 043902 (2003).
23. L. Mandel, E. Wolf, *Optical Coherence and Quantum Optics* (Cambridge Univ. Press, Cambridge, 1995).
24. Materials and methods are available as supporting material on *Science* Online.
25. Q. A. Turchette, R. J. Thompson, H. J. Kimble, *Appl. Phys. B* **60**, S1 (1995).
26. H. J. Kimble, M. Dagenais, L. Mandel, *Phys. Rev. Lett.* **39**, 691 (1977).
27. H. J. Carmichael, *Phys. Rev. Lett.* **55**, 2790 (1985).
28. D. K. Armani *et al.*, *Nature* **421**, 925 (2003).
29. H. J. Kimble, *Phys. Rev. Lett.* **90**, 249801 (2003).
30. L.-M. Duan, H. J. Kimble, *Phys. Rev. Lett.* **92**, 127902 (2004).
31. P. Treutlein *et al.*, *Fortschr. Phys. Progr. Phys.* **54,** 702 (2006).
32. G. Khitrova *et al.*, *Nat. Phys.* **2**, 81 (2006).
33. A. J. Shields, *Nat. Photon.* **1**, 215 (2007).

34. We gratefully acknowledge the contributions of S. Kelber, J. Petta, C. Regal, and E. Wilcut-Connolly. This research is supported by NSF, the Intelligence Advanced Research Projects Activity, and Northrop Grumman Space Technology.

Supporting Online Material

www.sciencemag.org/cgi/content/full/319/5866/1062/DC1
Materials and Methods
Figs. S1 to S4
References

29 October 2007; accepted 9 January 2008
10.1126/science.1152261

Downloaded from www.sciencemag.org on September 23, 2012